Faraday Discussions

Cite this: *Faraday Discuss.*, 2023, **245**, 508

ROYAL SOCIETY OF CHEMISTRY

PAPER

View Article Online
View Journal | View Issue

A systematic mechanistic survey on the reactions between OH radical and CH_3OH on ice†

W. M. C. Sameera, *[ab] Avon P. Jayaweera, [b] Atsuki Ishibashi, [a] Hiroshi Hidaka, [a] Yasuhiro Oba [a] and Naoki Watanabe [a]

Received 8th February 2023, Accepted 17th March 2023
DOI: 10.1039/d3fd00033h

A systematic mechanistic survey was performed for the CH_3OH + OH reaction on ice. ONIOM(ωB97X-D/Def2-TZVP:AMOEBA09) calculations suggested a range of binding energies for the CH_2OH radical (0.29–0.69 eV) and CH_3OH (0.15–0.72 eV) molecule on hexagonal water ice (I_h) and amorphous solid water (ASW). Computed average binding energies of CH_2OH radical (0.49 eV) and CH_3OH (0.41 eV) are relatively stronger compared to the CH_3O radical binding energies (0.32 eV, Sameera *et al.*, *J. Phy. Chem. A*, 2021, **125**, 387–393). Thus, the CH_3OH molecule, CH_2OH and CH_3O radicals can adsorb on ice, where the binding energies follow the order CH_2OH > CH_3OH > CH_3O. The multi-component artificial force-induced reaction (MC-AFIR) method systematically determined the reaction mechanisms for the CH_3OH + OH reaction on ice, where two reaction paths, giving rise to CH_2OH and CH_3O radicals, were confirmed. A range of reaction barriers, employing the ωB97X-D/Def2-TZVP level of theory, was found for each reaction (0.03–0.11 eV for CH_2OH radical formation, and 0.03–0.44 eV for CH_3O radical formation). Based on the lowest energy reaction paths, we suspect that both reactions operate on ice. The computed data in this study evidence that the nature of the binding site or the reaction site has a significant effect on the computed binding energies or reaction barriers. Thus, the outcomes of the present study will be very useful for the computational astrochemistry community to determine reliable binding energies and reaction barriers on ice.

Introduction

Radical species in the interstellar medium (ISM) play a key role in forming complex organic molecules (COMs).[1–8] The radicals in the ISM, such as the primary radicals (H, OH, CO, HCO, CH_3O, CH_2OH, CH_3, NH, and NH_2)[9,10] can be

[a]*Institute of Low Temperature Science, Hokkaido University, Sapporo, Hokkaido 060-0819, Japan. E-mail: wmcsameera@lowtem.hokudai.ac.jp*

[b]*Department of Chemistry, University of Colombo, Colombo 00300, Sri Lanka*

† Electronic supplementary information (ESI) available. See DOI: https://doi.org/10.1039/d3fd00033h

formed through surface reactions and the photodissociation of small molecules in interstellar ice. At very low temperatures (*e.g.*, 10 K), radical species adsorb on ice grain surfaces. Among the primary radicals, only H can diffuse on the ice at 10 K. The other primary radicals may start migrating on the ice at relatively high temperatures, the so-called warming-up stage. When a radical species encounters another radical or a molecule on ice, relatively large radicals or molecules can be formed. Therefore, quantitative details of the radical adsorption, radical diffusion, and radical reactions on ice are essential to understand the mechanisms of COMs formation. The radical processes on ice are challenging to characterize from experimental methods. Thus, computational studies are indispensable.[11]

Quantum mechanics (QM) and quantum mechanics/molecular mechanics (QM/MM) methods, typically employing density functional theory (DFT), allow fast and accurate determination of potential energy surfaces (PES) of complex molecular systems.[11–13] Then, the properties of the molecular systems, radical binding energy, reaction barriers, diffusion barriers, and reaction mechanisms can be calculated. We have used QM and QM/MM methods to calculate the binding energy of radical species on ice. The radical species interact with the dangling hydrogen (d-H) or dangling oxygen (d-O) on ice. Depending on the combination of dangling atoms at the binding site on ice, a range of binding energies was found for OH (0.06–0.74 eV),[14] HCO (0.12–0.42 eV),[14] CH_3 (0.11–0.26 eV),[14] CH_3O (0.10–0.50 eV),[15] PH_2 (0.16–0.21 eV),[16] PH (0.12–0.16 eV),[16] P (0.07–0.15 eV),[16] OCSH (0.19–0.46 eV).[17] We have also calculated radical reactions on ices; PH_3 + D,[16] and OCS + H,[17] and CH_3SH + H,[18] where the computed reaction mechanisms explained the experimental results.

CH_3OH is one of the molecules in the ISM that plays a crucial role in COMs formation. Thus, the formation of CH_3OH in the ISM and the reactions between CH_3OH and the primary radicals are very important. The successive hydrogenation of CO, an abundant molecule in the ISM, gives rise to CH_3OH (Scheme 1).[19,20] The first hydrogenation yields the HCO radical, and the second hydrogenation gives rise to the H_2CO molecule. CH_3O or CH_2OH radicals are the products of the third hydrogenation. Final hydrogenation gives CH_3OH. Among the three intermediate radicals in the mechanism, only the CHO and CH_3O radicals were found in the ISM.[21–23]

Reactions between the CH_3OH and OH radical, an abundant primary radical in the ISM, is a major interest to the astrochemistry field. Two reaction mechanisms have been proposed for the CH_3OH + OH reaction in the gas phase or on ice (Scheme 2). When CH_3OH and an OH radical come closer, $OH\cdots CH_3OH$ complex, a spectroscopically characterized complex,[24] is formed. According to *ab initio* computations on the gas phase reaction, CH_2OH radical formation [*i.e.*, reaction (i)] has a relatively low energy barrier, where quantum tunnelling plays a key role.[25–29] Another theoretical survey suggested that the cross-section yielding the CH_3O radical is higher than that for the CH_2OH radical.[27] The computed branching ratios at low temperatures and low pressure suggested that the CH_2OH

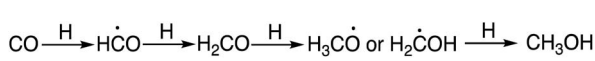

Scheme 1 Mechanism of CH_3OH formation through successive hydrogenation of CO.

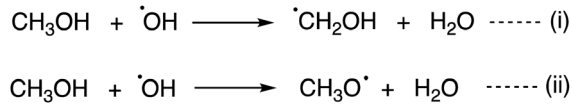

Scheme 2 Reaction mechanisms for the reaction between CH_3OH and the OH radical.

radical remains,[28] while below 40 K, the computed branching ratio was uncertain and sensitive to the computational methodology. Thus, outcomes of the reaction (*i.e.*, CH_2OH or CH_3O) at low temperatures are currently under active discussion. Recently, the importance of this reaction on ice dust was also proposed.[30]

In the present study, we calculated the binding energy of the CH_2OH radical and CH_2OH molecule on ice, employing a number of binding sites, and compared it with the binding energy of the CH_3O radical on ice.[15] Then, reaction mechanisms between CH_3OH and an OH radical on the ice were systematically determined.

Computational methods and models

Binding energy

Ice cluster models were taken from our previous study[15] to replicate amorphous solid water (ASW) and crystalline water ice (I_h) (Fig. 1). The ASW model has 162 H_2O molecules, where 50 H_2O molecules are in the QM region, and 112 H_2O molecules are in the MM region. The I_h models B and C, have 162 and 168 H_2O molecules, respectively. The QM region of model B has 48 H_2O molecules, and the MM region has 114 H_2O molecules. In model C, the QM and MM regions have 156 and 112 H_2O molecules, respectively.

Geometry optimizations were performed using the two-layer ONIOM method as implemented in the PyQM/MM interface.[31] The ωB97X-D,[32] functional and def2-TZVP,[33] basis sets were used for the ONIOM,[34,35] high-layer. The AMOEB09 [36–38] polarizable force field was used for the ONIOM low-layer. To avoid structure deformations, atoms in the ONIOM-low layer were frozen during the structure optimization. Vibrational frequency calculations were performed for the optimized structures to calculate the zero-point energy and to confirm the local

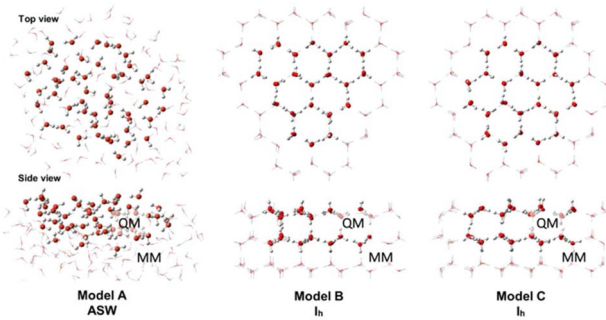

Fig. 1 Top and side views of the ice cluster models. The QM region is shown with "ball and stick" illustration, and the MM region is shown in "wireframe" illustration.

minima (*i.e.*, no imaginary frequencies). Binding energies were calculated using the following formula;

$$\text{Binding energy} = |E_{(\text{ice-molecule/radical})} - E_{\text{ice}} - E_{\text{molecule/radical}}|$$

where $E_{(\text{ice-molecule/radical})}$ is the total energy of the optimized CH_3OH-ice or CH_2OH-ice complexes. The E_{ice} term is the total energy of an optimized ice model system. The $E_{\text{molecule/radical}}$ is the energy of optimized CH_3OH or CH_2OH.

Reaction mechanisms

Reaction mechanisms between a CH_3OH molecule and an OH radical on ASW were determined by using the multi-component artificial force-induced reaction (MC-AFIR)[13,39] method as implemented in the GRRM17 program.[40] For this purpose, an ice cluster model, consisting of 76 H_2O molecules, was employed. In this model, 28 H_2O molecules on the side and bottom walls were frozen during the structure optimization, as highlighted in green in Fig. 2a and b, and the remaining 48 H_2O molecules were left flexible. The ωB97X-D method and the 6-31G* basis sets,[41–44] were used for the AFIR calculations. The CH_3OH molecule and OH radical were placed randomly on the ice surface. Then, an artificial force parameter of 100 kJ mol^{-1} was added between the CH_3OH and OH radical (Fig. 2c). After that, the resulting reaction paths (*i.e.*, AFIR paths), were inspected and approximate transition states (TSs) were identified, and fully optimized using the ωB97X-D/6-31G* level of theory, as implemented in the Gaussian16 program.[45]

Starting from the TS optimized structures, Pseudo intrinsic reaction coordinate calculations (IRC)[46,47] were performed for 20 steps forward and 20 steps backward from the optimized TS structures. Then, the local minima (LM) connecting the TSs (*i.e.*, the reactant complex and product) were calculated. Vibrational frequency calculations were performed to confirm that the optimized LM have no imaginary frequency and the optimized TSs have one imaginary frequency; and to calculate zero-point energies. Potential energies of the optimized LM or TSs were calculated as the single-point energy using the ωB97X-D/def2-TZVP level of theory.

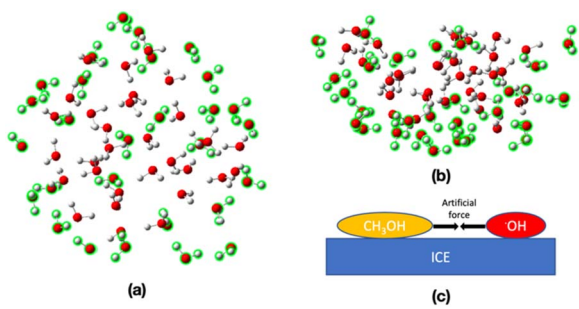

Fig. 2 (a) Top and (b) side views of the ice cluster model employed in this study. The water molecules highlighted in green were frozen during the structure optimization. (c) Adding artificial force between the CH_3OH and OH radical on ASW.

Results and discussion

Binding energy of CH_2OH and CH_3OH on ice

We have chosen 16 binding sites, eight from I_h (A–H) and eight from ASW (I–P) ice cluster models, to calculate binding energies. The computed binding energies are shown in Fig. 3. The molecular structures of the optimized structures are shown in Fig. S1 and S2.† The computed binding energies of the CH_2OH radical are in the range 0.29–0.69 eV, and the average binding energy is 0.49 eV (Fig. 3a). In the case of CH_3OH, the computed binding energies are in the range 0.15–0.72 eV, and the computed average binding energy is 0.41 eV (Fig. 3b).

Based on the average binding energies, we concluded that CH_2OH radical binding energy on ice is larger than that of the CH_3OH radical. From our previous study, using the same computational methods, we found that the average binding energy of the CH_3O radical is 0.32 eV.[15] Thus, the binding energy of the CH_3OH molecule, CH_2OH radical, and CH_3O radical follows the order CH_3O (0.32 eV) < CH_3OH (0.41 eV) < CH_2OH (0.49 eV). Therefore, if CH_3OH, CH_2OH, and CH_3O are formed on ice, the thermal desorption probability of these species would follow the opposite order, CH_3O < CH_3OH < CH_2OH.

In our ice models, a relatively large MM region is chosen. To check whether the MM region has a significant effect on the computed binding energies, we have compared binding energies (without ZPE) from ONIOM(ωB97X-D/Def2-TZVP:AMOEBA09) and ωB97X-D/Def2-TZVP methods (Fig. 4). In the case of the CH_2OH radical, the R^2 value of the plot is 0.99, indicating good agreement

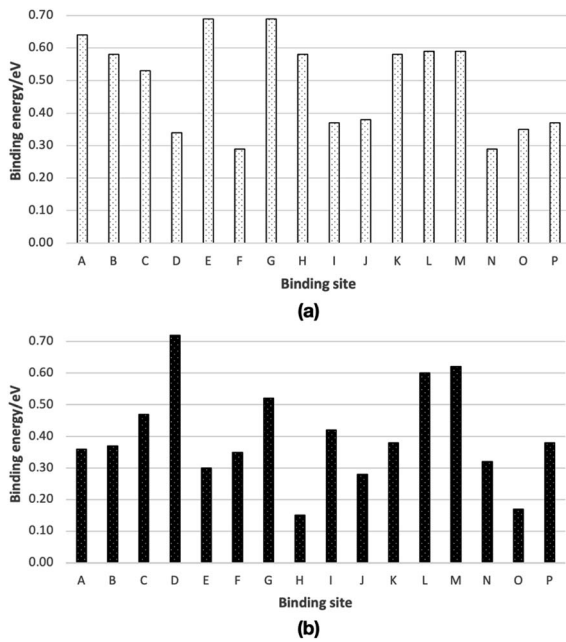

Fig. 3 Calculated binding energies of (a) a CH_2OH radical and (b) a CH_3OH on ice, from ONIOM(ωB97X-D/Def2-TZVP:AMOEBA09) calculations. Optimized molecular structures are shown in Fig. S1 and S2.† Binding energies are summarized in Table S1.†

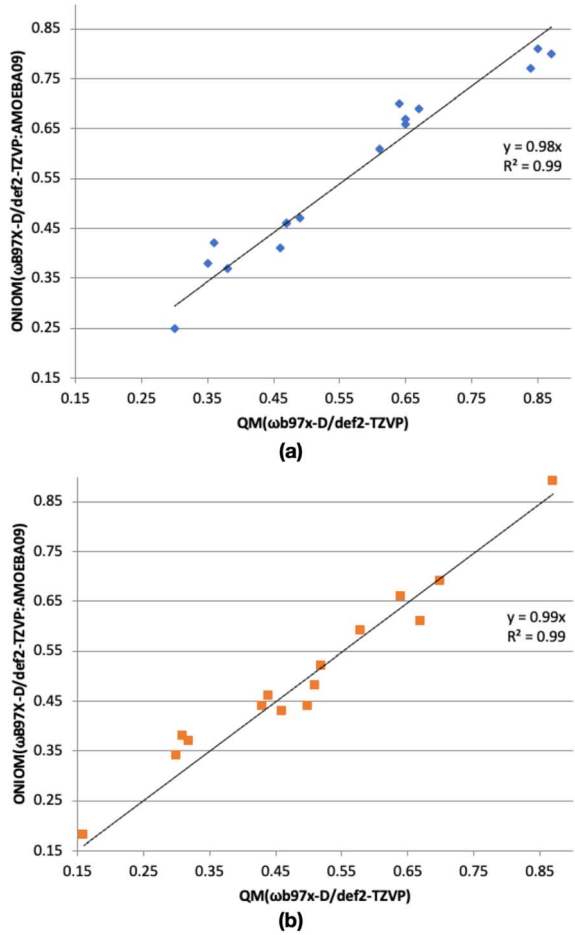

Fig. 4 ONIOM(ωB97X-D/def2-TZVP:AMOEBA09) binding energy (without ZPE) *vs.* ωB97X-D/def2-TZVP binding energy (without ZPE) of (a) CH_2OH radical, and (b) CH_3OH. Intercept of the linear trendlines were set to 0.0.

between the ONIOM(QM:MM) and QM binding energies. Similarly, the R^2 value of the plot of CH_3OH of 0.99, shows the good agreement between the computed binding energies from the ONIOM(ωB97X-D/Def2-TZVP:AMOEBA09) and ωB97X-D/Def2-TZVP methods.

The maximum discrepancy of the CH_2OH radical binding energies (without ZPE, Table S2†) of 0.07 eV of binding site A, is very small compared the computed binding energy of A, 0.77 eV. When we consider the lowest binding energy (0.25 eV), the discrepancy between the computed binding energy from ONIOM(ωB97X-D/Def2-TZVP:AMOEBA09) and ωB97X-D/Def2-TZVP methods is also small (0.05 eV). Thus, in general, binding energies from ONIOM(QM:MM) and QM methods are in agreement. Similarly, the maximum discrepancy of the CH_3OH radical binding energies (without ZPE, Table S2†) is 0.06 eV, belonging to binding sites E and N with the computed binding energy of 0.38 and 0.37 eV, respectively. If we consider the lowest binding energy of CH_3OH (0.18 eV, binding site H), the

discrepancy between the computed binding energy from ONIOM(QM:MM) and QM methods is very small (0.02 eV). Therefore, the ONIOM(QM:MM) method gave reliable binding energies.

In the present study, it is important to note that we have chosen 16 binding sites to calculate binding energies. Thus, we were able to cover a number of arrangements of the dangling atoms at the binding sites, where the interactions between the radical and the binding site are diverse, allowing us to collect a range of binding energies.

CH_3OH + OH reaction on ice

This section focuses on the mechanisms for the reaction between CH_3OH and an OH radical on ice. An MC-AFIR search was performed to determine reaction paths systematically, and two reaction paths were found on ice; (a) $CH_3OH + OH \rightarrow CH_2OH + H_2O$ and (b) $CH_3OH + OH \rightarrow CH_3O + H_2O$. We have chosen four AFIR paths for each reaction mechanism and potential energy surfaces were calculated (Fig. 5). The lowest and highest computed potential energy barrier for the CH_2OH radical formation is 0.03 eV and 0.11 eV, respectively (Fig. 5a), and therefore the computed reaction barrier is in a range. Similarly, the computed potential energy barrier for the CH_3O radical formation is also in a range (Fig. 5b), where the lowest energy barrier is 0.03 eV, while the highest barrier is 0.44 eV. If the lowest energy

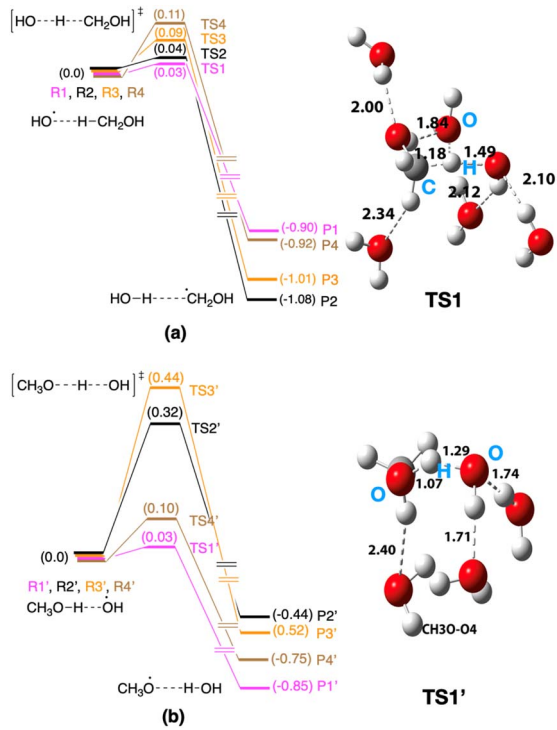

Fig. 5 Computed potential energy surfaces for (a) $CH_3OH + OH \rightarrow CH_2OH + H_2O$ and (b) $CH_3OH + OH \rightarrow CH_3O + H_2O$ reactions. Optimized transition state structures are shown in Fig. S3 and S4†).

reaction path is taken into account (*i.e.*, 0.03 eV for the formation of the CH_2OH radical and 0.03 eV for the formation of the CH_3O radical), both reaction mechanisms may operate on ice. In the case of the products of the reactions, the CH_2OH radical is thermodynamically more stable compared to the CH_3O radical in all cases. Further, if we take the lowest energy paths of the two mechanisms, the HO–H$\cdots$$CH_2OH$ complex is −1.08 eV more stable compared to the entry point of the potential energy profile, while the HO$\cdots$$CH_3O$ complex is −0.85 eV more stable compared to its entry point.

In this reaction path survey, we restricted the analysis to four reaction paths for each reaction (eight reaction paths in total). Even with these data, we can see a range of reaction barriers for each reaction. If we extend the analysis for collecting more reaction paths, we suspect that the reaction barrier range will be broadened. The lowest barrier limit is the key to the rate of the reaction. In this present case, both reactions operate at a very low reaction barrier of 0.03 eV. Therefore, both reaction mechanisms would operate on interstellar ice.

Conclusions

We have used the ONIOM(ωB97X-D/def2-TZVP:AMOEBA09) method to calculate CH_2OH and CH_3OH radical binding on ASW and I_h. A range of binding energies were found for each species; CH_3OH: 0.15–0.72 eV; CH_2OH: 0.29–0.69 eV. Thus, both CH_2OH and CH_3OH radicals would adsorb on interstellar ice. The calculated average binding energies, 0.41 eV of CH_3OH and 0.49 eV of CH_2OH, indicate the strong binding preference of CH_2OH, and are relatively stronger compared to the CH_3O radical binding energies (0.32 eV).[15] Reaction paths for the CH_3OH + OH were searched using the MC-AFIR method. Two reaction mechanisms were determined, giving rise to CH_2OH and CH_3O products. A range of reaction barriers was found for each reaction mechanism; 0.03–0.11 eV for the CH_2OH radical formation and 0.02–0.44 eV for the CH_3O radical formation. Both radicals can be formed on ice if the lowest energy paths are taken into account. As radical binding on ice and radical reactions on ice cover a range of numbers, a systematic sampling of binding energies or reaction barriers becomes critical, which is the key lesson we have learned from this study.

Author contributions

WMCS designed the project, performed calculations, and wrote the original manuscript with help from APJ. AI, HH, YO and NW performed the experiments relevant to this study. All co-authors have revised the manuscript and given approval to the final version of the manuscript.

Conflicts of interest

There are no conflicts to declare.

Acknowledgements

This work was partly supported by the JSPS KAKENHI grant numbers JP19K03940 (to WMCS), JP21H05416 (to WMCS), JP17H06087 (to NW), and JSPS grant number

JPJSBP 120229901 (to WMCS). Supercomputing resources at the Institute for Information Management and Communication at Kyoto University in Japan and the Institute for Molecular Science (IMS) in Japan are also acknowledged.

References

1 E. Herbst and E. F. Van Dishoeck, *Annu. Rev. Astron. Astrophys.*, 2009, **47**, 427–480.
2 S. Bottinelli, C. Ceccarelli, J. P. Williams and B. Lefloch, *Astron. Astrophys.*, 2007, **463**, 601–610.
3 E. Herbst and R. T. Garrod, *Front. Astron. Space Sci.*, 2022, **8**, 1–6.
4 A. Bacmann, V. Taquet, A. Faure, C. Kahane and C. Ceccarelli, *Astron. Astrophys.*, 2012, **541**, L12–5.
5 C. Vastel, C. Ceccarelli, B. Lefloch and R. Bachiller, *Astrophys. J.*, 2014, **795**, L2–11.
6 R. T. Garrod, S. L. W. Weaver and E. Herbst, *Astrophys. J.*, 2008, **682**, 283–302.
7 K. I. Öberg, E. F. Van Dishoeck, H. Linnartz and S. Andersson, *Astrophys. J.*, 2010, **718**, 832–840.
8 K. J. Chuang, G. Fedoseev, S. Ioppolo, E. F. van Dishoeck and H. Linnartz, *Mon. Not. R. Astron. Soc.*, 2016, **455**, 1702–1712.
9 R. T. Garrod, S. L. W. Weaver and E. Herbst, *Astrophys. J.*, 2008, **682**, 283–302.
10 K. Öberg, E. F. van Dishoeck, H. Linnartz and S. Andersson, *Astrophys. J.*, 2010, **718**, 832–840.
11 W. M. C. Sameera, B. Senevirathne, T. Nguyen, Y. Oba, A. Ishibashi, M. Tsuge, H. Hidaka and N. Watanabe, *Front. Astron. Space Sci.*, 2022, **9**, 890161.
12 W. M. C. Sameera and F. Maseras, *Wiley Interdiscip. Rev.: Comput. Mol. Sci.*, 2012, **2**, 375–385.
13 W. M. C. Sameera, S. Maeda and K. Morokuma, *Acc. Chem. Res.*, 2016, **49**, 763–773.
14 W. M. C. Sameera, B. Senevirathne, S. Andersson, F. Maseras and G. Nyman, *J. Phys. Chem. C*, 2017, **121**, 15223–15232.
15 W. M. C. Sameera, B. Senevirathne, S. Andersson, M. Al-Lbadi, H. Hidaka, A. Kouchi, G. Nyman and N. Watanabe, *J. Phys. Chem. A*, 2021, **125**, 387–393.
16 T. Nguyen, Y. Oba, W. M. C. Sameera, A. Kouchi and N. Watanabe, *Astrophys. J.*, 2021, **918**, 73.
17 T. Nguyen, Y. Oba, W. M. C. Sameera, A. Kouchi and N. Watanabe, *Astrophys. J.*, 2021, **922**, 146.
18 T. Nguyen, Y. Oba, W. M. C. Sameera, A. Kouchi and N. Watanabe, *Astrophys. J.*, 2023, **944**, 219.
19 A. G. G. M. Tielens and W. Hagen, *Astron. Astrophys.*, 1982, **114**, 245–260.
20 N. Watanabe and A. Kouchi, *Astrophys. J.*, 2002, **571**, L173–L176.
21 J. Cernicharo, N. Marcelino, E. Roueff, M. Gerin, A. Jiménez-Escobar and G. M. Caro, *Astrophys. J.*, 2012, **759**, L43.
22 L. E. Snyder, J. M. Hollis and B. L. Ulich, *Astrophys. J.*, 1976, **208**, L91–L94.
23 V. M. Rivilla, M. T. Beltrán, A. Vasyunin, P. Caselli, S. Viti, F. Fontani and R. Cesaroni, *Mon. Not. R. Astron. Soc.*, 2019, **483**, 806–823.
24 F. J. Hernandez, J. T. Brice, C. M. Leavitt, G. A. Pino and G. E. Douberly, *J. Phys. Chem. A*, 2015, **119**, 8125–8132.

25 S. Blázquez, D. González, A. García-Sáez, M. Antiñolo, A. Bergeat, F. Caralp, R. Mereau, A. Canosa and B. Ballesteros, *ACS Earth Space Chem.*, 2019, **3**, 1873–1883.
26 R. J. Shannon, M. A. Blitz, A. Goddard and D. E. Heard, *Nat. Chem.*, 2013, **5**, 745–749.
27 O. Roncero, A. Zanche and A. Aguado, *Phys. Chem. Chem. Phys.*, 2018, **20**, 25951–25958.
28 A. J. Ocaña, S. Blázquez, A. Potapov, B. Ballesteros, A. Canosa, M. Antiñolo, L. Vereecken, J. Albaladejo and E. Jiménez, *Phys. Chem. Chem. Phys.*, 2019, **21**, 6942–6957.
29 L. G. Gao, J. Zheng, A. Fernández-Ramo, D. G. Truhlar and X. Xu, *J. Am. Chem. Soc.*, 2018, **140**, 2906–2918.
30 A. Ishibashi, H. Hidaka, Y. Oba, A. Kouchi and N. Watanabe, *Astrophys. J.*, 2021, **921**, L13.
31 M. Rathnayake, W. M. C. Sameera and N. Watanabe, *ChemRxiv*, 2022, preprint, DOI: **10.26434/chemrxiv-2022-2c8mz**.
32 J.-D. Chai and M. Head-Gordon, *Phys. Chem. Chem. Phys.*, 2008, **10**, 6615–6620.
33 F. Weigend and R. Ahlrichs, *Phys. Chem. Chem. Phys.*, 2005, **7**, 3297–3305.
34 W. M. C. Sameera and F. Maseras, *J. Chem. Inf. Model.*, 2018, **58**, 1828–1835.
35 L. W. Chung, W. M. C. Sameera, R. Ramozzi, A. J. Page, M. Hatanaka, G. P. Petrova, T. V. Harris, X. Li, Z. Ke, F. Liu, H.-B. Li, L. Ding and K. Morokuma, *Chem. Rev.*, 2015, **115**, 5678–5796.
36 J. W. Ponder and D. A. Case, Force Fields for Protein Simulations, *Adv. Protein Chem.*, 2003, **66**, 27–85.
37 P. Ren and J. W. Ponder, *J. Comput. Chem.*, 2002, **23**, 1497–1506.
38 P. Ren and J. W. Ponder, *J. Phys. Chem. B*, 2003, **107**, 5933–5947.
39 W. M. C. Sameera, A. K. Sharma, S. Maeda and K. Morokuma, *Chem. Rec.*, 2016, **16**, 2349–2363.
40 S. Maeda, Y. Harabuchi, M. Takagi, K. Saita, K. Suzuki, T. Ichino, Y. Sumiya, K. Sugiyama and Y. Ono, *J. Comput. Chem.*, 2018, **39**, 233–251.
41 R. Ditchfield, W. J. Hehre and J. A. Pople, *J. Chem. Phys.*, 1971, **54**, 724–728.
42 W. J. Hehre, R. Ditchfield and J. A. Pople, *J. Chem. Phys.*, 1972, **56**, 2257–2261.
43 P. C. Hariharan and J. A. Pople, *Theor. Chim. Acta*, 1973, **28**, 213–222.
44 M. M. Francl, W. J. Pietro, W. J. Hehre, J. S. Binkley, M. S. Gordon, D. J. DeFrees and J. A. Pople, *J. Chem. Phys.*, 1982, **77**, 3654–3665.
45 M. J. Frisch, G. W. Trucks, H. B. Schlegel, G. E. Scuseria, M. A. Robb, J. R. Cheeseman, G. Scalmani, V. Barone, G. A. Petersson, H. Nakatsuji, X. Li, M. Caricato, A. V. Marenich, J. Bloino, B. G. Janesko, R. Gomperts, B. Mennucci, H. P. Hratchian, J. V. Ortiz, A. F. Izmaylov, J. L. Sonnenberg, D. Williams-Young, F. Ding, F. Lipparini, F. Egidi, J. Goings, B. Peng, A. Petrone, T. Henderson, D. Ranasinghe, V. G. Zakrzewski, J. Gao, N. Rega, G. Zheng, W. Liang, M. Hada, M. Ehara, K. Toyota, R. Fukuda, J. Hasegawa, M. Ishida, T. Nakajima, Y. Honda, O. Kitao, H. Nakai, T. Vreven, K. Throssell, J. A. Montgomery Jr., J. E. Peralta, F. Ogliaro, M. J. Bearpark, J. J. Heyd, E. N. Brothers, K. N. Kudin, V. N. Staroverov, T. A. Keith, R. Kobayashi, J. Normand, K. Raghavachari, A. P. Rendell, J. C. Burant, S. S. Iyengar, J. Tomasi, M. Cossi, J. M. Millam, M. Klene, C. Adamo, R. Cammi, J. W. Ochterski, R. L. Martin, K. Morokuma, O. Farkas,

J. B. Foresman and D. J. Fox, GAUSSIAN 16 (Revision C.01), Gaussian, Inc., Wallingford, CT, 2016.
46 K. Fukui, *Acc. Chem. Res.*, 1981, **14**, 363–368.
47 H. P. Hratchian and H. B. Schlegel, *Theory and Applications of Computational Chemistry, The First Forty Years*, 2005, pp. 195–249.

